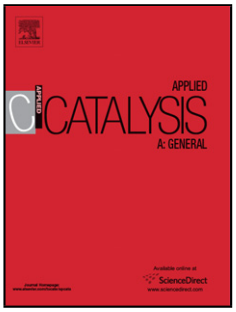

Title: New synthetic route for the production of mayenite support to enhance Ni resistance to coke deposition in the reforming of tar model compounds

Authors: M.P. Bracciale, B. de Caprariis, P. De Filippis, A.D. Hernandez, M. Scarsella

PII: S0926-860X(19)30051-1
DOI: https://doi.org/10.1016/j.apcata.2019.01.029
Reference: APCATA 16969

To appear in: *Applied Catalysis A: General*

Received date: 30 November 2018
Revised date: 27 January 2019
Accepted date: 29 January 2019

Please cite this article as: Bracciale MP, de Caprariis B, De Filippis P, Hernandez AD, Scarsella M, New synthetic route for the production of mayenite support to enhance Ni resistance to coke deposition in the reforming of tar model compounds, *Applied Catalysis A, General* (2019), https://doi.org/10.1016/j.apcata.2019.01.029

New synthetic route for the production of mayenite support to enhance Ni resistance to coke deposition in the reforming of tar model compounds.

M.P. Bracciale, B. de Caprariis, P. De Filippis, A.D. Hernandez*, M. Scarsella

Department of Chemical Engineering Materials Environment, Sapienza University of Rome, via Eudossiana 18, 00184 Rome, Italy

Graphical abstract

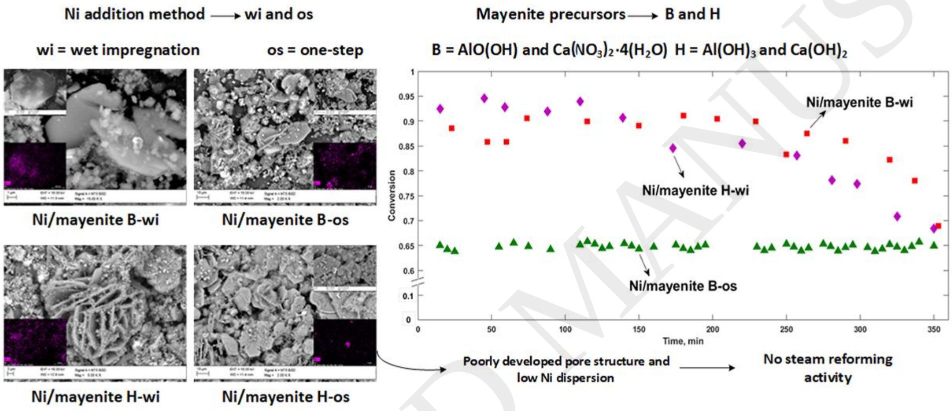

Highlights

- Mayenite carriers were synthesized by two innovative routes using different precursors, $AlO(OH) + Ca(NO_3)_2$ and $Al(OH)_3 + Ca(OH)_2$.
- Nickel addition to the carriers was performed via wet impregnation and a one-step method during the mayenite preparation.
- The catalyst prepared with the one-step method and using $AlO(OH) + Ca(NO_3)_2$ as precursors showed promising tolerance to deactivation by carbon deposition.
- Different nickel-support interactions due to the applied nickel addition method were verified by TPR analysis.

ABSTRACT

Four nickel/mayenite catalysts were synthesized. Mayenite was prepared from different precursors, namely boehmite (AlO(OH)) + $Ca(NO_3)_2 \cdot 4H_2O$ and gibbsite + $Ca(OH)_2$, for each couple a specific procedure was followed. The effect of the Ni addition method was also evaluated, comparing wet impregnation and direct inclusion of nickel precursor during mayenite preparation. The obtained catalysts were characterized by XRD, BET, SEM/EDS and TPR. The Ni/mayenite catalysts were tested in steam reforming of toluene and pyrocatechol, chosen as tar model compounds. The experiments were conducted in a fixed-bed lab-scale atmospheric reactor, evaluating carbon conversion, hydrogen selectivity and stability. Characterization of the spent catalysts after toluene steam reforming experiments by XRD and DTG-TPO were performed to assess structural changes and carbon deposition. Kinetic parameters of toluene steam reforming were determined for the different catalysts

Keywords: mayenite; steam reforming; nickel; tar model compounds; on-step synthesis; catalyst characterization

1. Introduction

Biomass has the potential to partly replace fossil fuels via syngas generation through gasification and subsequent conversion of the produced syngas to green-fuels, energy and chemicals [1,2]. However, the presence of deleterious contaminant species at concentrations detrimental to most downstream applications hinders the utility of biomass derived syngas [3]. Among the by-products of biomass gasification tar species pose the greatest problem to end users. Tar is defined as all hydrocarbons with a molecular weight higher than benzene, which at high temperatures (≥ 700 °C) mainly includes aromatic compounds with a condensation temperature ranging between 150 and 300 °C [4,5]. If not removed from the produced syngas, tar compounds could block downstream pipelines and foul engines and turbines causing unsustainable penalties on the profitability of the plant. Therefore, the removal and/or conversion of these contaminants represents a critical step to exploit efficiently and sustainably the valuable gases present in the syngas.

In spite of the extensive effort devoted to reduce the concentration of tar species inside the gasifier to the actual stringent values required for downstream applications, the results are still far from satisfactory [6]. Hence the use of cleaning and conditioning technologies downstream the gasifier is crucial to adhere to the requirements of end users. Amid those strategies, the catalytic steam reforming reaction is a promising solution because it has the potential to increase the amount of valuable gases such as H_2, CO and CH_4 present in the syngas while reducing the waste streams generated using the classic wet cold gas cleaning technologies[7]. Additionally, it can take advantage of the high temperature of the syngas at the gasifier exit.

The majority of commercial steam reforming plants from 1950 to 2009 exploited nickel-based catalysts [7] and nickel is still the most common active metal used nowadays. This can be ascribed to the optimum balance between nickel cost and catalytic reforming activity. Nevertheless, deactivation by carbon deposition is still an unsolved issue that has negative consequences on the operational costs [8].

Many efforts for suppressing carbon formation on Ni catalysts have been undertaken, and it has been shown that the use of thermal-stable supports featuring high amount of “free” oxygen species can enhance the carbon deposition resistance of nickel catalysts [9–11]. A pioneering work on the production of H_2 from catalytic steam reforming of bio-oil conducted by Wang et al. [12] tested the unique O^- storage and emission behavior of mayenite ($C_{12}Al_{14}O_{33}$). The authors speculated that the high initial activity of the Mg/mayenite catalyst could be attributed to reactions of the vaporized bio-oil with the active O^- species present in the mayenite structure.

Mayenite has a unique cubic crystal structure composed of three-dimensionally connected sub-nanometer-sized cages where 2 out of 12 cages are statistically occupied by O^{2-} and O^- ions to compensate the positive charge of the cage framework having the chemical composition of $[Ca_{24}Al_{28}O_{64}]^{4+}$ [13]. These anions feature a nearly free mobility within the cage. Hosono et al. [13] found many evidences of the possible replacement of the free O^{2-} with OH^-, O_2^-,O^- by tuning the atmosphere during the heat treatment. Boysen et al. [14] by means of a high-temperature neutron powder diffraction study showed that at high temperature the mobility of the “free” oxygen species increased significantly in the mayenite structure due to a jump-like process which involve the exchange of “free” oxygen with oxygen species from the mayenite framework. Based on these findings it is believed that during the steam reforming reaction these “free” oxygen species in the mayenite lattice will migrate to nickel site to gasify the carbon deposited on nickel catalyst, reducing the carbon deposition on the active sites [9].

Li et al. [9] used Ni/mayenite for the steam reforming of toluene obtaining promising results in terms of resistance to carbon formation and tolerance to sulfur containing species. Di Carlo et al. [15] studied the steam reforming activity of a Ni/mayenite catalyst using a microreactor fed by a slipstream coming from a bench-scale fluidized-bed biomass gasifier. The catalyst maintained a high conversion (≈0.9) of heavy hydrocarbons for 12 h at 800 °C. The above referenced studies prepared the mayenite support using different methods. Li et al. [9] used $Ca(OH)_2$ and $Al(OH)_3$ as precursors applying the solid-state reaction method, whereas Di Carlo et al. [15] worked in slurry employing $Ca(CH_3COO)_2$ mixed with Al_2O_3.

In the present work, two different synthetic routes using different precursors to produce mayenite were investigated and compared. The Ni/mayenite catalysts with a Ni loading of 10 wt% were obtained by wet impregnation or one-step inclusion during the carrier synthesis. The catalysts were tested in the steam reforming of tar model compounds i.e. toluene and pyrocatechol, as representatives of aromatic stable compounds and oxygenated aromatic compounds, respectively. Additionally, characterization of the synthesized mayenite support and catalysts was conducted to correlate the structural, morphologic and topologic features of the samples with their steam reforming performance.

2. Experimental

2.1. Supports and catalysts syntheses

Mayenite, used as support in all the catalysts, was obtained starting from different precursors: from boehmite ($AlO(OH)$) and $Ca(NO_3)_2{\cdot}4H_2O$ (termed in this study mayenite B) and from gibbsite ($Al(OH)_3$) and $Ca(OH)_2$ (termed mayenite H).

Mayenite B was synthetized starting from a stable dispersion of boehmite [16]. First a dispersion was prepared adding commercial aluminum oxide hydroxide powder (Sigma Aldrich ≥ 99.0 %) to a 0.4 % (w/w) HNO_3 aqueous solution and then $Ca(NO_3)_2{\cdot}4H_2O$ (Sigma Aldrich ≥ 99.0 %)was added to the dispersion under vigorous stirring. The used amount of $Ca(NO_3)_2{\cdot}4H_2O$ was determined based on the stoichiometric ratio in the mayenite (Ca/Al molar ratio = 12/14). The dispersion was kept under stirring for 24 h at room temperature until a gel was obtained. The gel was then dried overnight at 100 °C and the resultant solid was grinded and calcined at 950 °C for 16h under static air.

For the synthesis of mayenite H, $Al(OH)_3$ (Sigma Aldrich, reagent grade) and $Ca(OH)_2$ (Sigma Aldrich ≥ 99.9 %) were stoichiometrically mixed in solid state, then water was added until a homogeneous dense slurry was obtained. The slurry was dried for 24 h at 105 °C, then the obtained solid was grinded and calcined at 1250 °C for 16 hours under static air.

The calcination temperature for mayenite B and H was determined based on TGA-DSC analysis (SDTQ600, TA instrument) performed on the precursors, where the exothermic peak of the phase transformation was recorded at 940 °C and 1250 °C for boehmite and hydroxides precursors, respectively (Fig. S1).

Four nickel supported catalysts were prepared with two different routes for the metal addition on mayenite B and H. The first route was by wet impregnation (wi) on the previously obtained supports (Ni/mayenite B-wi and Ni/mayenite H-wi) sieved between 0.1-0.3 mm. These solids were mixed under stirring with the aqueous solution of Ni precursor and then dried for 24 h at 105 °C. The powders obtained were calcined at 900 °C for 6 h under static air atmosphere.

The second route was by a “one step” (os) procedure consisting in adding the Ni precursor directly during the mayenite preparation procedures described above. In the case of Ni/mayenite B-os the Ni precursor was added to the dispersion together with calcium precursor, while to prepare Ni/mayenite H-os the Ni precursor was dissolved in the water added to the mixture of solid precursor to obtain a dense slurry.

In all the cases $Ni(NO_3)_2{\cdot}6H_2O$ (Sigma Aldrich 99.99 %)was used as precursor and its amount was calculated to produce a catalyst having 10 wt. % of nickel.

2.2. Experimental set-up

The experimental setup used for the steam reforming of toluene (STR) and pyrocathecol (SPR) is depicted in Fig. 1. The detailed description of the set-up is reported in [11].

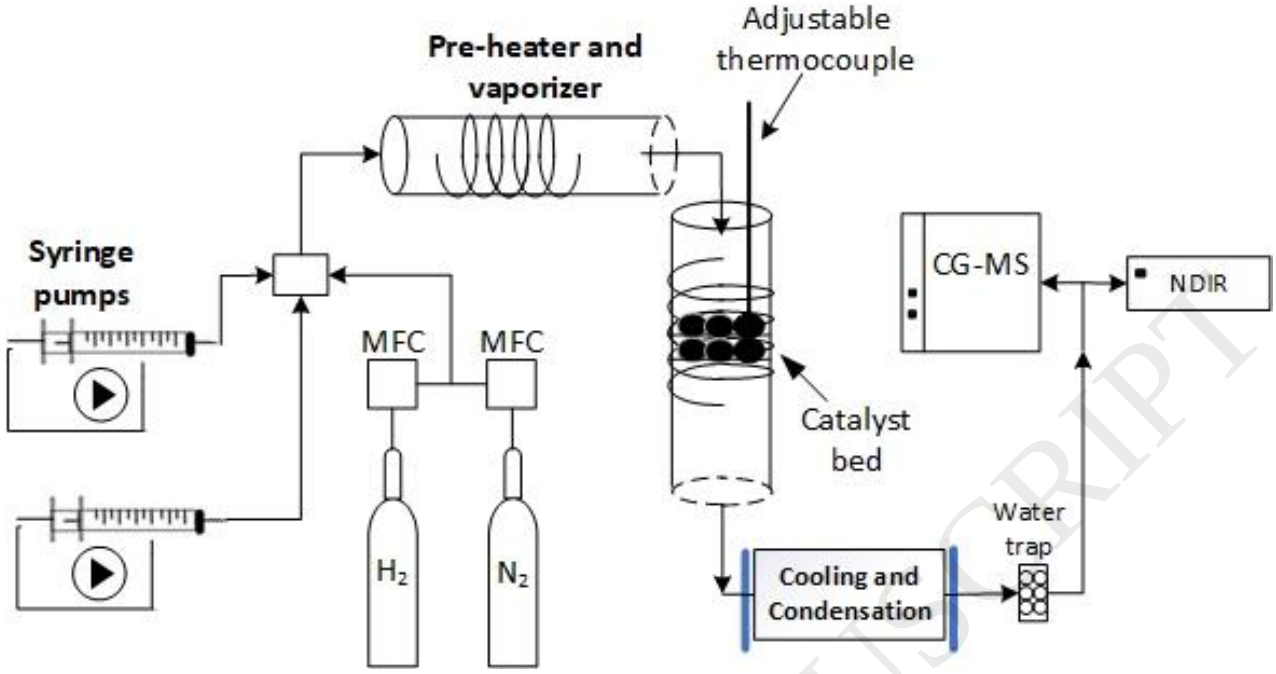

Fig. 1. Experimental set-up.

The reagents used in this study were deionized water, toluene (Sigma-Aldrich ≥ 99.5 %) and pyrocatechol (Sigma-Aldrich ≥ 99.0 %). During the STR, toluene and water were fed separately to the reactor, whereas in the case of SPR, pyrocatechol was dissolved in deionized water in the appropriate steam to carbon ratio (S/C) before feeding the solution to the reactor. In both cases N_2 was employed as carrier gas; the reagent mixture was sent to an evaporator held at 300 °C before it entered to the reactor. The catalysts were held by a small piece of quartz wool placed on top of a stainless-steel grid. In each experiment 0.1 g of catalyst (grain size 0.1-0.3 mm) mixed with 1 g of SiO_2 (grain size 0.1-0.3 mm) was used. The height of the bed was 15 mm. At the reactor exit the unreacted species and condensable products were recovered in a counter-current condenser using water maintained at 5 °C by means of a chiller. The produced gas flow was measured with a volumetric flow meter. CO, CO_2 and CH_4 were measured by an online analyzer (Siemens Ultramat 21). A fixed bed of small Al_2O_3 sticks were placed before the on-line analyzers to adsorb any residual steam content present in the gas. The concentration of H_2 and possible traces of C_2H_4 were determined using a GC mass spectrometer (Hiden QGA). Before the experiments the prepared catalysts were activated in situ at 700 °C for 30 min in 0.5 NL min^{-1} of 16 % H_2/N_2 and then held at 750 °C for 1h in N_2 flow 0.24 Nl min^{-1}. At the end of each test the heating system was turned off and the catalyst was cooled down under N_2 to room temperature, then it was collected and kept in a glass sealed container.

To evaluate the activity of the SiO_2 filler material on the conversion of the tar model compounds a pure SiO_2 bed was used in the reactor and experiments with the model tar compounds were performed at 750 °C keeping constant all the experimental conditions used for the catalytic tests. The concentration values of

CO and H_2 measured at the reactor exit were negligible, hence the catalytic/thermal effect of the reactor and the SiO_2 particles was neglected.

The occurrence of deactivation was evaluated conducting 6 h long tests at 700 °C

The experimental conditions used are reported in Table 1. In the present work severe conditions with respect to the inlet tar concentration were used, these conditions are comparable with the tar concentration measured in atmospheric bubbling fluidized bed biomass gasifiers with steam as gasifier agent [17]. The chosen S/C ratio was based on reported values of syngas composition obtained in air [18] and steam/oxygen [17] fluidized bed gasifiers. In addition, the relatively high S/C value was applied to prevent a fast deactivation of the catalysts due to carbon deposition during the tests conducted to obtain the kinetics parameters

Table 1
Experimental conditions used in the experimental tests

	STR	SPR
Temperature (°C)	670-750	670-750
Total gas inlet flow (NL min^{-1})	0.41	0.41
N_2 flow rate (NL min^{-1})	0.24	0.24
Tar model compound concentration (g Nm^{-3})	47	65
GHSV (h^{-1} at 700 °C)	73750	73900
Space-time, $W_{cat}/F_{toluene}$ (kg_{cat} h Nm^{-3})	0.33	0.28
S/C	5	5

2.3. Catalyst characterization

The obtained catalysts and supports were analysed by X-ray powder diffraction (XRPD) (Philips Analytical PW1830), Brunauer-Emmett-Teller (BET) and Barrett-Joyner-Halenda (BJH) analyses. XRD patterns were acquired using a Philips Analytical PW1830 X-ray diffractometer, equipped with Cu Kα (1.54056 Å) radiation, in the 2θ range from 15 to 70° with a step size of 0.02° and a time for step of 3.5 s. The data were collected with an acceleration voltage and applied current of 40 kV and 30 mA, respectively. The crystalline phases in the resulting diffractograms were identified through the COD database (Crystallography Open Database – an open-access collection of crystal structures) [19]. The average nickel crystallite sizes were calculated with the Scherrer's equation on the most intense Ni peak plane.

BET analyses were determined by N_2 adsorption–desorption isotherms acquired at −196°C using a Micromeritics Triflex analyzer (Micromeritics Instrument Corp.). The adsorption-desorption isotherms were acquired in the p/p^0 range from 0.01 to 0.99. Isotherm analyses were performed using the 3Flex Version 4.05 software. Samples were previously outgassed at 300 °C for 3 h. The BET and BJH equations were used to determine the specific surface area, pore volume and average pore diameter, respectively.

In order to obtain morphologic and topologic information, SEM/EDS (Scanning Electron Microscopy combined with Energy Dispersive X-ray Spectrometry) analysis were performed on the obtained catalysts. Backscattered electron (BSE) images were recorded with a High Resolution-Field Emission Scanning

Electron Microscope (HR-FESEM, AURIGA Zeiss) operated at 15 kV. The samples were prior sputter-coated with 10 nm thin layer of chromium using a Quorumteach Q150T sputter coater. For elemental analyses EDS maps were acquired with QUANTAX EDS XFlash® 6 detector (Bruker Nano GmbH), providing elemental topography of zones of external surfaces.

Ni/mayenite reducibility properties of the fresh catalysts were measured by temperature-programmed reduction (TPR) experiments with a thermogravimetric analyzer SDTQ600 (TA Instruments, USA). The samples were pre-treated under Ar flow at 150 °C for 60 min to remove adsorbed moisture and air. Then the TPR profiles were recorded by heating the sample from 40 °C to 900 °C at 5 °C min^{-1} under a H_2 flow (5.0 % H_2 in Ar, 50 mL min^{-1}).

The carbon deposited content was determined by Thermogravimetric (TG) analysis using an SDTQ600 simultaneous TGA- DSC analyzer (TA Instruments, USA) under a gas mixture of 20 % O_2 in nitrogen and with a flux rate of 100 mL min^{-1}. The samples were prior heated under nitrogen in an open ceramic pan up to 800 °C with a ramp rate of 20 °C min^{-1} in order to strip away volatile organic compounds physically absorbed and to thermally decompose any carbonatic species produced on spent catalysts during reaction. The samples were then equilibrated to 31 °C and the O_2/N_2 gas mixture was introduced. Specimens were afterward subjected to the following thermal program: heating up to 230 °C, 30 min hold, heating to 800 °C and 30 min hold, all ramps at 10 °C min^{-1}.

2.4. Carbon conversion and H_2 selectivity

A simplified reaction scheme which considers only the steam reforming and the water gas shift (WGS) reactions was adopted for the steam reforming processes [20]:

$$\mathrm{STR} = \mathrm{C_7H_8 + 7H_2O \rightarrow 7CO + 11H_2} \tag{1}$$

$$\mathrm{SPR} = \mathrm{C_6H_6O_2 + 4H_2O \rightarrow 6CO + 7H_2} \tag{2}$$

$$\mathrm{WGS} = \mathrm{CO + H_2O \leftrightarrow CO_2 + H_2} \tag{3}$$

The conversion of the tar model compounds was calculated as the carbon conversion X_C:

$$X_C = \frac{n_{CO_{OUT}} + n_{CO2_{OUT}} + n_{CH4_{OUT}}}{\text{molar flow of carbon in the feed}} \tag{4}$$

where $n_{CO_{OUT}}$, $n_{CO2_{OUT}}$, and $n_{CH4_{OUT}}$ are the molar flow of gas containing carbon at the reactor exit, i.e. CO, CO_2 and CH_4, respectively. Reactions leading to carbon formation on the catalyst such as toluene decomposition and the Boudouard reaction are expected to proceed concurrently with the steam reforming and WGS reactions and need to be considered.

Hydrogen selectivity was calculated according to the work of Polychronopoulou et al. [21]:

$$S_{H_2} = \frac{y_{H_2}}{b * y_{CO} + c * y_{CO_2}} \tag{5}$$

S_{H_2} was used to identify whether reactions other than those described in the selected reaction network occurred [21]. y_{H_2}, y_{CO} and y_{CO_2} are the measured mole fractions of hydrogen, CO and CO_2, respectively, at the exit of the reactor. In equation (5) the coefficients b and c represent the stoichiometric correlation of 1 mol of hydrogen to that of the produced CO and CO_2, respectively, based on reactions (1) and (3) for toluene and (2) and (3) in the case of pyrocatechol.

2.5. Kinetics: Evaluation of mass transfer limitation

Axial isothermal conditions were checked during the experiments using the adjustable thermocouple inside the catalyst bed. Temperature and concentration gradients within the particles were assumed to be negligible because of the low surface area of the used catalyst (see Table 2) [22]. The occurrence of external mass transfer limitation was excluded by calculation of the Mears' criterion [23].

A selected number of experiments with fresh catalysts and using toluene as model tar compound were dedicated to obtaining kinetic parameter in which fresh catalyst was used in every experiment. Four different temperatures were set in each test. The same catalyst was used for the whole duration of the test. The experiments were performed starting from the lowest temperature. Each selected temperature was maintained until the concentration of the main gases reached steady state conditions, usually 20 min, after which the temperature was increased.

Plug flow condition was checked using the criteria proposed by Froment et al. [24]. The ratio of the height of the bed to the particle size was larger than the criterion for axial dispersion i.e. catalyst bed height/particle diameter ≥ 50. The ratio of the internal diameter of the reactor and the catalyst particle was higher than 30 and hence the channeling criterion was fulfilled.

The apparent kinetic parameters were carried out assuming a pseudo first-order reaction with respect to the tar model compound and being independent from H_2O concentration as the latter was fed in excess. This assumption have been widely accepted in the literature [25,26]. The reaction rate was calculated as follow:

$$-r_{app} = k_{app} * C_{tar} \tag{6}$$

Under conditions very close to plug flow, the mass balance for the tar compound gives:

$$k_{app} = \frac{-\ln(1-X_C)}{\tau} \tag{7}$$

where r_{app} is the rate of conversion (kmol m^{-3} h^{-1}), k_{app} is the apparent kinetic constant (m^3 (Tcat. N_2-free) kg^{-1} h^{-1}), C_{tar} is the tar model compound concentration (kmol m^{-3}), X_C is the carbon conversion, and τ is the residence time in the catalyst bed that was calculated as follows:

$$\tau = \frac{W_{cat}}{Q_{in}(\text{Tcat.})} \tag{8}$$

where W_{cat} is the catalyst weight (kg) and $\mathrm{Q_{in}(Tcat.)}$ is the inlet volume flow rate at the catalyst bed temperature after subtracting the N_2 flow (m^3 h^{-1}), with this units of measurement the obtained $\mathrm{k_{app}}$ is thus calculated at the catalyst temperature and without considering the N_2 flow rate. This was done to compare the results with the reported data of Aznar et al. [26].

The apparent kinetic constant ($\mathrm{k_{app}}$) of tar model compounds were calculated using the carbon conversion $\mathrm{X_C}$ (Eq. 4) and therefore the obtained $\mathrm{k_{app}}$refers to all the reactions involved in the formation of CO, CO_2 and CH_4.

2.6. Thermodynamic calculations

Thermodynamic equilibrium calculations were done using Aspen plus V8.8®. The Gibbs reactor was chosen to calculate the equilibrium composition of the simulated gas. The SRKKD thermodynamic method was set for all the calculations. The input for the simulation was the set molar flow rates of C_7H_8, water and N_2. The following vol. % dry composition of the gas was obtained at 700 °C: H_2 = 21.2 %, CO = 2.7 %, CO_2 = 6.6 % and $CH_4 = 4.0 \times 10^{-3}$. Complete carbon conversion was achieved at 700 °C. Moreover, carbon conversion was 0.99 at the lowest temperature used in this study i.e. 620 °C. The influence of the excess of steam on the WGS reaction and thus on the equilibrium H_2 vol. % value that can be obtained considering only the steam reforming (SR) and WGS reactions was explored using the equilibrium reactor of Aspen plus V8.8® with the same thermodynamic method as in the Gibbs reactor case. First the simulation was run setting only the SR reaction. Next a second run was done but this time both the WGS and SR reaction were set. The difference in the H_2 vol. % of the two simulations was due to the WGS reaction induced by the excess of steam. The share of the WGS reaction on the equilibrium H_2 vol. % value decreased from 27 to 25 % when the temperature increased from 620 to 740 °C

3. Results and discussion

3.1. Fresh catalyst characterization

XRD patterns of the synthetized catalysts are shown in Fig. 2.

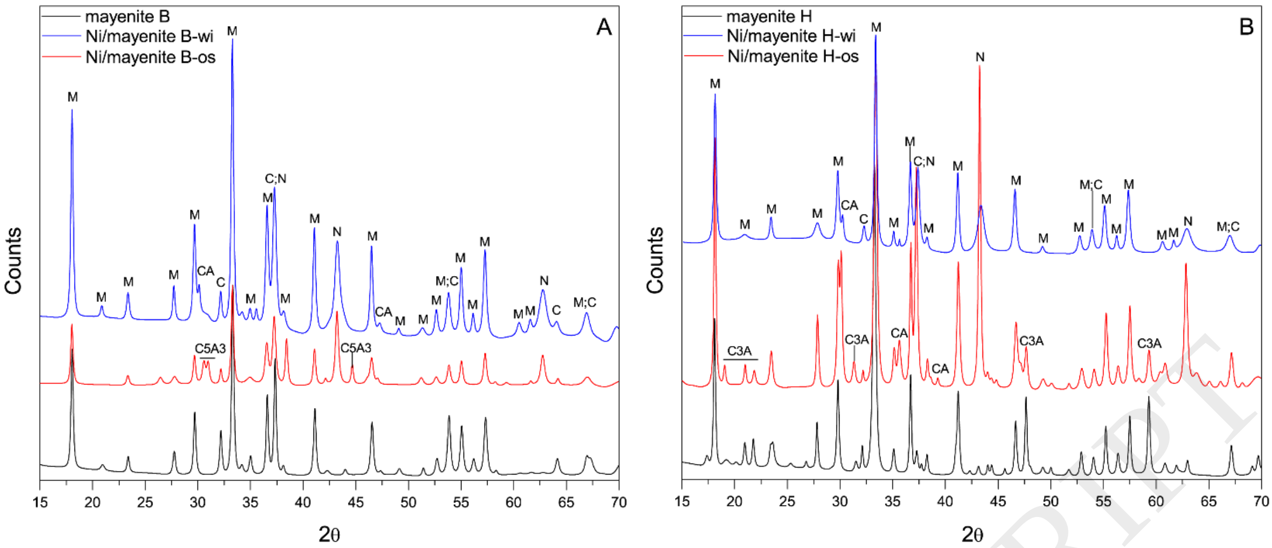

Fig. 2. XRD patterns of mayenite synthetized by boehmite (A) and hydroxides (B) precursors. M ($Ca_{12}Al_{14}O_{33}$); C (CaO); N (NiO); CA ($CaAl_2O_4$); C3A ($Ca_3Al_2O_6$); C5A3 ($Ca_5Al_6O_{14}$).

The main crystal structures of both supports (mayenite B and mayenite H) were similar despite of the different precursor used. The characteristic reflections of the {211} and {420} planes of crystalline $Ca_{12}Al_{14}O_{33}$ (18.1° and 33.3°) [27–29] and CaO (32.2°, 37.3°, 64.1°) can be distinguished. Furthermore, in the case of mayenite H (Fig. 2B) diffraction rays corresponding to $Ca_3Al_2O_6$ (C3A) at 2θ angles of 20.9°, 21.7°, 47.6° and 45.5° were clearly detected. The presence of CaO was probably due to segregation of the Ca during the preparation [28,29], instead $Ca_3Al_2O_6$ is a high temperature (930-1330 °C) intermediate of mayenite formation. This latter exhibits wide crystals that prevent the formation of mayenite [30]. Furthermore, as previously reported, this phase is common when powder reactants that lead to a heterogeneous mixture are used [31]. After Ni nitrate addition and calcination, neither $NiAl_2O_4$ spinel phase nor hydrated structures $Ca(OH)_2$ or formation of solid solution between NiO and CaO were identified. The Ni/mayenite catalysts showed the characteristic reflections of crystalline NiO at 43.2° and 62.8°. The wet impregnation method led in both the cases to the formation of a little amount of $CaAl_2O_4$ phase probably due to the hydration and subsequent calcination stages used during the preparation. This phase was detected in larger amount in the Ni/mayenite H-os sample. Instead the Ni/mayenite B-os catalyst showed the doublet belonging to $Ca_5Al_6O_{14}$ (C5A3) at 2θ = 30.6 and 31.0°, which is recognized in the literature as the low temperature metastable phase (< 950 °C) in the Ca–Al–O system [31,32].

The diffraction patterns of catalysts after the in-situ activation (700 °C for 30 min in 0.5 NL min^{-1} of 16 % H_2/N_2 and then held at 750 °C for 1h) showed well defined diffraction rays of metallic nickel (see section 3.5). The average crystallite size of metallic nickel (Table 2) is about 20–22 nm and 38-71 nm for the samples prepared by wet impregnation and on-step method, respectively.

Table 2 shows the catalysts' surface area. The adsorption-desorption plots of all the catalysts showed type IV adsorption isotherms with an H1 hysteresis [33], denoting that the mesoporous structure of the support has not been modified by the insertion of Ni (Fig. S2-S3). The surface areas of the mayenite B catalysts (mayenite B, Ni/mayenite B-wi and Ni/mayenite B-os) were higher than those of mayenite H (mayenite H, Ni/mayenite H-wi and Ni/mayenite H-os). The decrease in the surface area could be attributed to collapse of the pores in the samples, which occurs with an increase in the temperature (1250 °C compared to 950 °C) that lead to a high compaction of the crystals, as demonstrated by SEM images (Fig. 3) and the lower pore volume values (Table 2). Furthermore, the catalysts obtained by wet impregnation method (Ni/mayenite B-wi and Ni/mayenite H-wi) exhibited surface areas relevantly bigger than their respective support (mayenite B and mayenite H). The increase in the surface area after impregnation could be due to the hydration stage used during the preparation. Indeed, as previously reported [34,35], the addition of the aqueous solution of nickel nitrate may lead to the formation of hexagonal $Ca(OH)_2$ that become porous CaO during the subsequent calcination step at 900 °C. Furthermore, the Ni insertion led to a general small increase of the surface area in all the catalysts, suggesting that the metallic nanoparticles did not fill the support's pore structure.

The obtained BET surface area values are in fair agreement with those reported in the literature , regardless of the preparation method used, the latter values ranging from 2.5 to 24.3 m^2 g^{-1} [9,28,35–37].

Table 2
BET-BJH data for fresh catalysts.

Catalysts	Crystal size (nm)[a]	BET Surface Area (m^2/g)[b]	Pore Volume (cm^3/g)[c]	Average Pore Diameter (nm)[d]
mayenite B	-	4.13	0.015	1.9
Ni/mayenite B-wi	20.7	12.92	0.027	12.6
Ni/mayenite B-os	37.9	4.53	0.009	1.9
mayenite H	-	0.24	0.0007	26.7
Ni/mayenite H-wi	21.7	6.82	0.027	17.9
Ni/mayenite H-os	70.5	0.60	0.0026	25.82

[a] by XRD using Scherrer equation on Ni {111} plane; [b] by BET equation; [c-d] by BJH desorption.

The morphological study of the obtained samples was carried out with SEM-EDS (Fig. 3). The mayenite B series consisted of well-defined laminar aggregates with nano-thickness ~50 nm. Ni/mayenite B-wi displayed NiO crystallites, not uniformly distributed on $Ca_{12}Al_{14}O_{33}$, as it is clear in Fig. 3. Ni/mayenite H-wi, instead, exhibited a microstructure of $Ca_{12}Al_{14}O_{33}$ formed by dendritical aggregates. The lower specific surface area and poorly developed pore structure of Ni/mayenite H-os effectively inhibited the dispersion of Ni active metal, as shown by EDS maps in Fig. 3. As a confirmation of the obtained XRD results, some cubic crystals of CaO were detected during the SEM analysis.

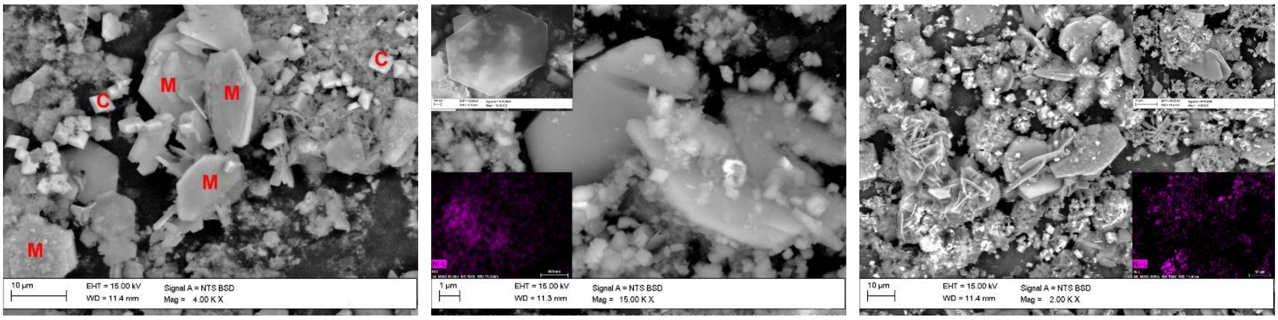

mayenite B Ni/mayenite B-wi Ni/mayenite B-os

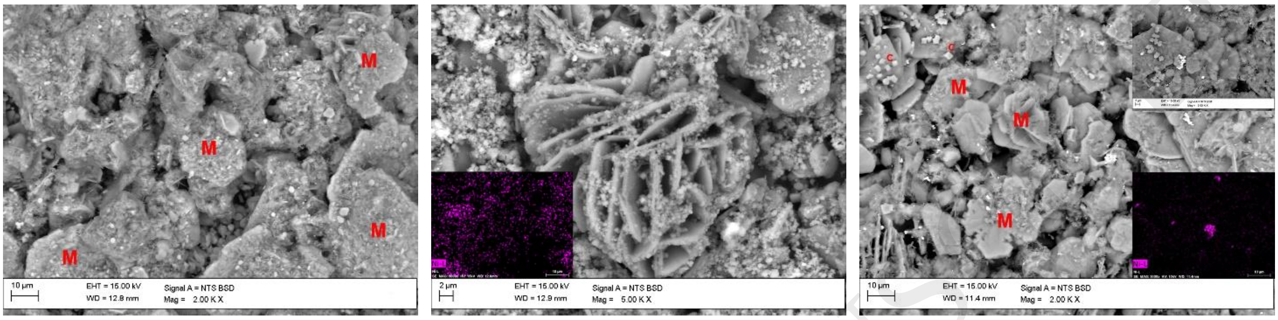

mayenite H Ni/mayenite H-wi Ni/mayenite H-os

Fig. 3. SEM micrographs showing the Ni dispersion on the synthetized catalysts. EDS maps of Ni are included as insets. M ($Ca_{12}Al_{14}O_{33}$); C (CaO).

TPR profiles of Ni/mayenite catalysts in Fig. 4 were used to estimate the Ni available for reduction. The reduction degree calculated considering the theoretical nickel loading is listed in Table 3.

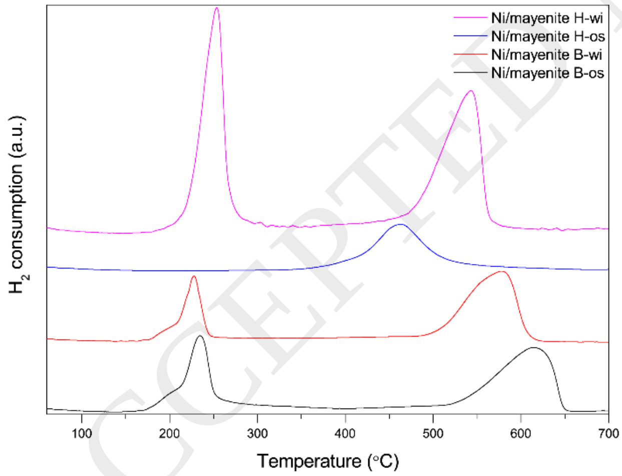

Fig. 4. H_2 consumption during TPR of catalysts

On all the catalysts the main H_2 consumption was observed in the temperature range between 150 and 650 °C. On Ni/mayenite B catalysts the main reduction peaks, observed around 230 and 615 °C, lead to a reduction degree of 66 and 63 % for Ni/mayenite B-wi and Ni/mayenite B-os, respectively. The peak at lower temperature could be ascribed to the reduction of isolated NiO particles [38,39] with smaller size and very finely distributed, which weakly interacted with or was far from the support and then were easier to reduce. For higher temperatures, the reduction peak at 615 °C (Ni/mayenite B-os) can be ascribed to a stronger interaction state of NiO with the mayenite support and CaO [40,41]. The area corresponding to the reduction of these latter Ni species is the largest among the peaks detected, denoting that Ni bonded to the mayenite support are the principal Ni species in this catalyst. As previous reported, the strong interaction of Ni^{2+} ions with the mayenite support reduces the mobility and agglomeration with other Ni particles on the surface [28]. The peaks were slightly shifted to lower temperature for the Ni/mayenite B-wi sample. Furthermore, the Ni-based reduction degree (Table 3) on the B-wi catalyst is higher than that on the B-os catalyst. This behavior can be interpreted as a consequence of the stronger interaction between Ni and mayenite introduced by the one step method. The highest reduction degree was obtained with the Ni/mayenite H-wi catalyst (83.23%). In this case the area associated with the low and high reduction temperature peaks were identical. From Table 3 it is possible to identify on this latter catalyst that the temperature and the H_2 consumption of the low temperature reduction peak were considerably higher than the corresponding values of the Ni/mayenite B catalysts. This result could be ascribed to higher content of isolated NiO particles in this catalyst as reported by Cabello et al. [39]. Furthermore, the high temperature reduction peak was shifted to lower temperatures with respect to the Ni/mayenite B catalysts, this result, as stated above, could suggest a weaker metal-support interaction. It is well documented [42–44] that the strong nickel-support interactions are beneficial for the enhancement of the catalysts stability and the carbon deposition tolerance. Considering the obtained TPR it is expected that the catalyst where the strongest Ni-support interactions were present was the Ni/mayenite B-os (Table 3). On the other hand, the reduction degree of Ni/mayenite H-os was only about 5%, probably due to the high calcination temperatures markedly decreasing the accessibility of nickel and thus its reducibility [25,45]. From the TPR profiles of the synthetized catalysts, the reduction temperature for catalysts testing was set at 700 °C, in order to reduce an important proportion of the Ni^{2+} species with weak and high interaction with the mayenite support.

Table 3

Catalyst properties after H_2 temperature-programmed reduction (TPR) experiments

Catalysts	Content (10^{-3} mol g_{cat}^{-1})	Main consumption peaks (°C)	H_2 consumption (10^{-3} mol g_{cat}^{-1})	Reduction degree [11] (%)
Ni/mayenite B-wi	1.7	228; 578	0.31; 0.81	66.0
Ni/mayenite B-os		235; 614	0.44; 0.64	63.31
Ni/mayenite H-wi		253; 543	0.71; 0.71	83.23
Ni/mayenite H-os		460	0.09	5.08

3.2. Steam Reforming of Toluene (STR)

Ni/mayenite H-os did not show any steam reforming activity at the experimental conditions used in the present work, thus it was not considered in the next sections. This outcome could be attributed to its unfavorable structural and morphological features, as discussed in section 3.1, which lead to a low reduction degree of Ni species (Table 3).

The conversion as a function of time-on-stream (ToS) at 700 °C is shown in Fig. 5. In the case of Ni/mayenite B-wi and Ni/mayenite H-wi a similar trend was observed. These catalysts exhibited high conversion values with a slight deactivation towards the end of the test. On the other hand, lower but stable values were obtained using Ni/mayenite B-os. The lower activity of the latter catalyst could be attributed to the higher nickel crystal size and/or due its lower reduction degree which is related to a lower amount of potential chemically actives sites and hence lower conversions. Contribution to the observed lower conversion by virtue of the degradation of the support and the presence of NiO after the tests as found during the characterization of the spent catalyst cannot be excluded (see section 3.5). After 6 h ToS analogous carbon conversion values were observed for the three catalysts.

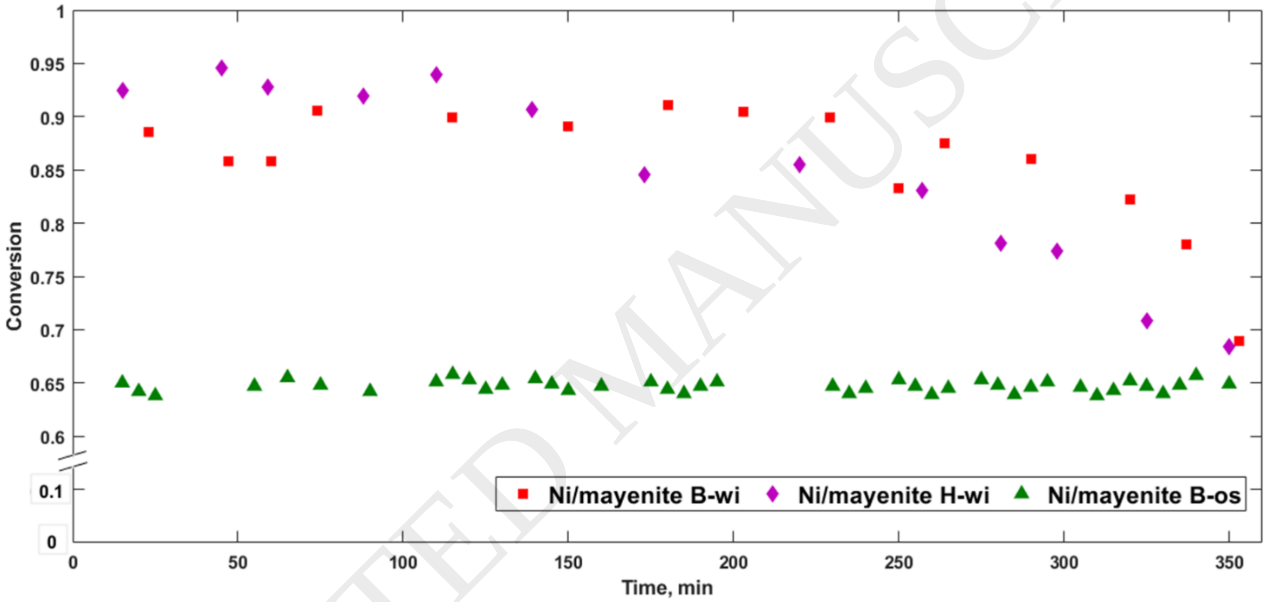

Fig. 5. Conversion as a function of time-on-stream for toluene steam reforming (700 °C; S/C =5)

In Fig. 6 S_{H_2} values are depicted as a function of time-on-stream (ToS) at 700 °C~~.~~ The S_{H_2} obtained values were proximate to 1 throughout the entire experiment, being slightly lower in the case of Ni/mayenite B-os. Based on these results it is safe to say that the extent of the reactions other than the complete steam reforming of toluene to carbon oxides and hydrogen was insignificant. Moreover, the activity decrease observed at the end of the test for Ni/mayenite B-wi and Ni/mayenite H-wi did not affect the S_{H_2} achieved with these catalysts.

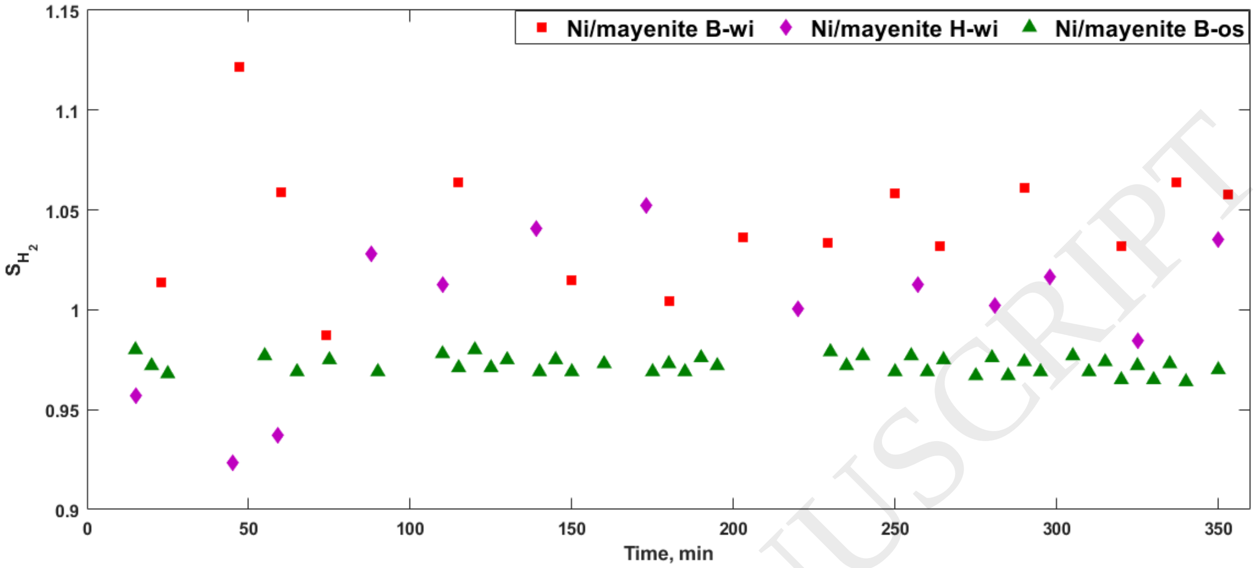

Fig. 6. Hydrogen selectivity parameter to identify whether reactions other than those described in the selected reaction network occurred for STR at 700 °C.

The conversion as a function of temperature is depicted in Fig. 7. As in the conversion as a function of ToS the Ni/mayenite B-wi and Ni/mayenite H-wi catalysts showed a comparable activity, besides the curves seemed to follow a linear behavior. A lower activity was observed for Ni/mayenite B-os as expected from the results obtained during the six hour-long tests. The latter catalyst needed higher temperature to equal the conversion values achieved with the catalysts synthesized by wet impregnation.

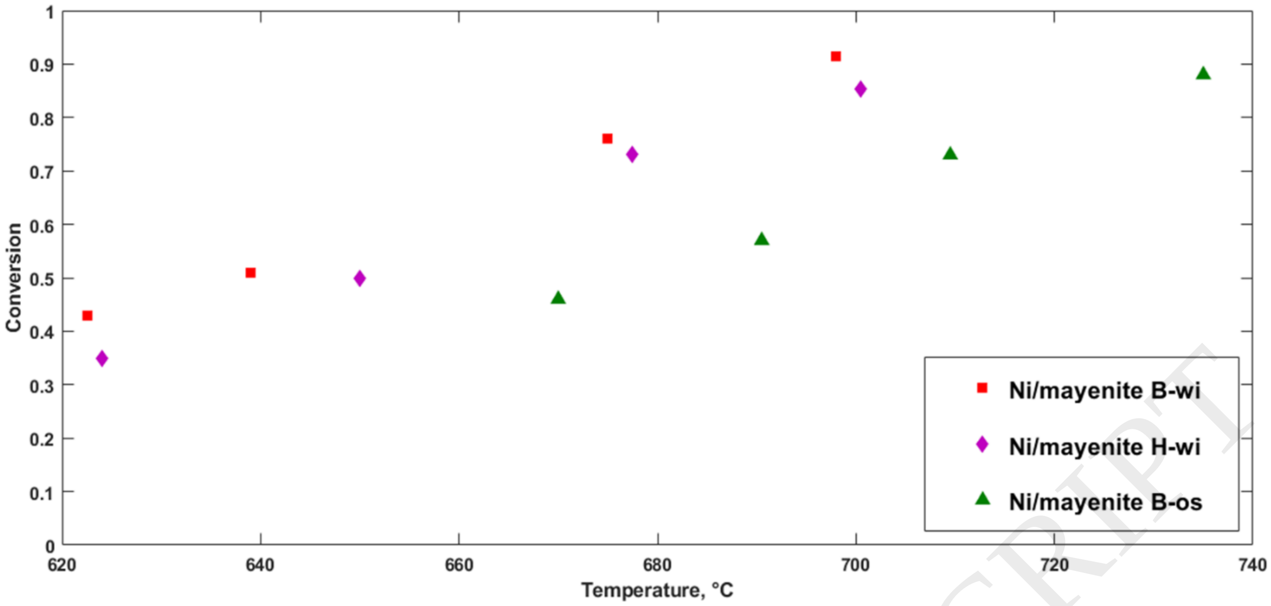

Fig. 7. Conversion as a function of temperature for toluene steam reforming (S/C=5).

Table 4 shows the measured gas volumetric flow rate (N_2-free basis), the concentration of H_2, CO and CO_2 and the calculated hydrogen selectivity S_{H_2} at three different temperatures for the three catalysts considered. As expected, the gas flow rate and the measured concentration of non-condensable gases increased with temperature. The highest CO_2 vol% values were obtained with Ni/mayenite B-os despite the higher temperature applied during the tests with this catalyst. This result could be ascribed to a higher WGS reaction activity of the catalyst synthesized with the one-step procedure. S_{H_2} values were close to 1 in all cases, hence, it can be assumed that in the studied operating conditions the extent of reactions forming or consuming hydrogen other than reactions (1) and (3) were negligible. The conversion and hydrogen selectivity data of the highest temperature is not reported in Table 4 and can be found in Fig. 5 and Fig. 6 as a function of time of stream for Ni/mayenite B-wi and Ni/mayenite H-wi, respectively.

As stated above from the equilibrium carbon conversion calculations almost complete carbon conversion was reached already at the lowest applied temperature of this study. From the experimental results showed in Figure 7 is evident that the tests were performed far from the equilibrium, specially the experiments done at temperatures ≤ 650 °C with the catalysts synthesized by the wet impregnation method. Additionally, considering the CO_2, CO and H_2 equilibrium values showed in Table 4 it can be concluded that the WGS reaction was far from equilibrium and was likely controlled by the kinetics of the process for the whole range of temperature applied.

Table 4
Total dry gas flow rate (N_2-free basis) and main non-condensable gases measured at the outlet of the reactor at different temperatures. The calculated equilibrium values for the non-condensable gases are listed for comparison.

	Ni/mayenite B-wi			Ni/mayenite H-wi			Ni/mayenite B-os		
Cat. Temperature (°C)	623	639	675	624	650	678	670	690	710
Total dry gas flow rate, N_2-free basis (Nl/min)	0.04	0.07	0.09	0.03	0.05	0.09	0.03	0.07	0.09
H_2 vol%	7.5	12.7	17.3	7.2	12.4	17.3	7.1	12.4	17.3
H_2 equilibrium vol%	21.6	21.6	21.4	21.6	21.5	21.4	21.3	21.2	21.0
CO_2 vol%	1.9	2.9	4.0	1.9	2.9	4.4	2.0	3.5	5.0
CO_2 equilibrium vol%	7.1	6.9	6.7	7.1	6.9	6.7	6.6	6.5	6.3
CO vol%	1.8	3.5	4.6	1.6	3.3	4.0	1.4	2.3	3.1
CO equilibrium vol%	2.1	2.3	2.6	2.2	2.4	2.6	2.7	2.9	3.1
S_{H_2}	0.97	0.98	0.99	0.98	0.98	0.98	0.96	0.98	0.98

3.3. *Steam Reforming of Pyrocatechol (SPR)*

The conversion as a function of time for the SPR at 700 °C is showed in Fig. 8. Conversion values were lower than those obtained at the beginning of the STR experiments (Fig. 5**Error! Reference source not found.**). The most stable catalyst was the Ni/mayenite B-os that, after a slight activity decrease, maintained a constant conversion of ca. 0.5 throughout the experiment. The other two catalysts presented a slow and steady deactivation. Koike et al. [47] did a comparative study on steam reforming of benzene, toluene and phenol over Ni and Ni-Fe alloy nanoparticles supported on a Mg/Al hydrotalcite at 600 °C and contact time W/F = 0.01 – 0.05 g h mol^{-1}. Lower conversions values and higher carbon deposition were observed on both catalysts when phenol was fed to the reactor compared to toluene and benzene. Stronger adsorption of phenol and its intermediates on the surface of the catalysts with respect to the other aromatic compounds was thought to be the reason for the results obtained.

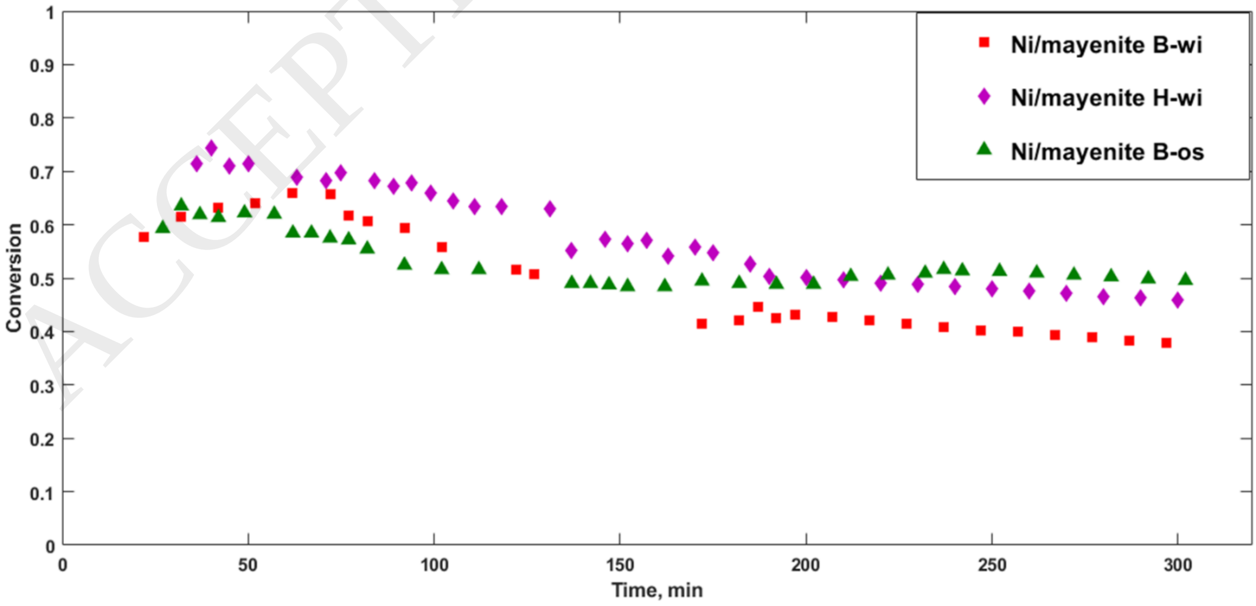

Fig. 8. Conversion as a function of time-on-stream for pyrocatechol steam reforming (700 °C ; S/C =5).

Hydrogen selectivity values S_{H_2} are illustrated in Fig. 9. As in the STR experiments the S_{H_2} curves where all in the immediacy of 1 and thus it was assumed that the main reactions taking place during the SPR experiments where those based on reactions (2) and (3), i.e. the total steam reforming.

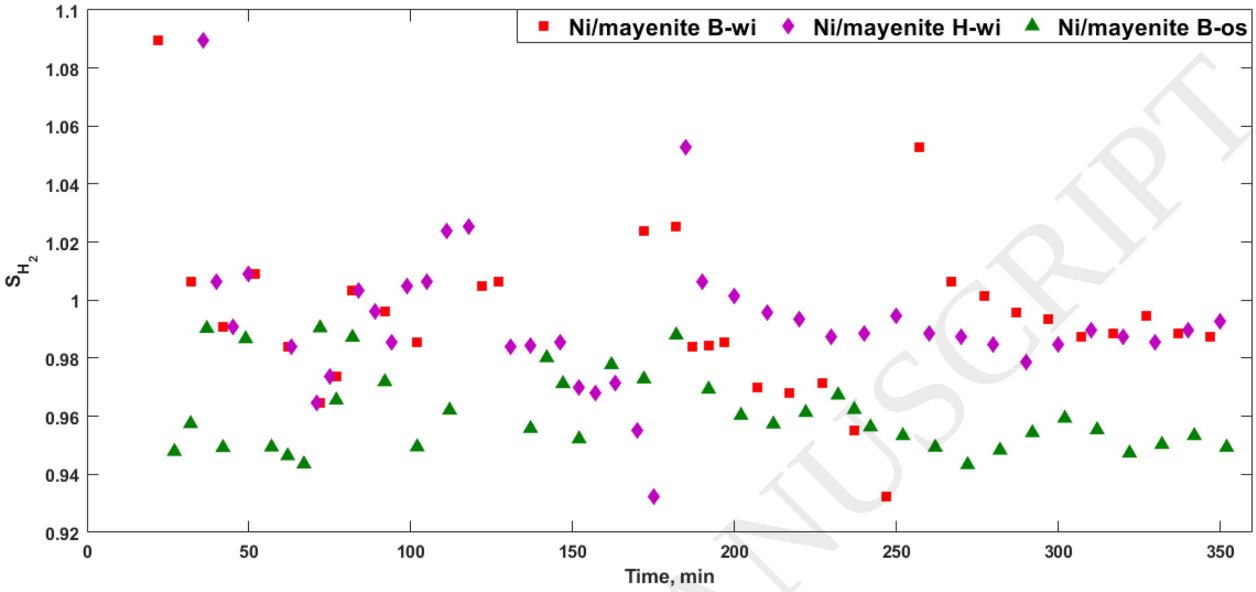

Fig. 9. Hydrogen selectivity parameter to identify whether reactions other than those described in the selected reaction network occurred for SPR (700 °C).

Interestingly, CH_4 was not detected during the steam reforming experiments carried out in the present study. Probably, the methanation reaction did not occur in the present catalytic system. Furthermore, it can be speculated that the extent of reactions forming methane e.g. hydrodealkylation, were negligible and/or the methane formed was converted to CO, CO_2 and H_2. According to Mukai et al. [48] the most abundant intermediate in the steam reforming reaction of toluene at 600 °C on a $Ni/La_{0.7}Sr_{0.3}AlO_{3-\delta}$ was C_2H_4. However, in the present study C_2H_4 was not detected in any of the tests. The results observed in the present study are in agreement with Świerczyński et al. [25] who observed only CO, CO_2 and H_2 when the catalyst temperature was ≥ 650 °C using a Ni/olivine catalyst during the STR with a space-time of 9 kg_{cat} h m^{-3} at 25 °C. Koike et al. [47] did not detect any traces of CH_4 after steam reforming of phenol at 600 °C over a Ni-Fe/Mg/Al catalyst

3.4. Kinetics

The k_{app} as a function of temperature for the STR is showed in Fig. 10. In the case of Ni/mayenite B-os the higher temperature at which the k_{app} values presented a sharp increment could be attributed to a different interaction between the support and the nickel active sites in comparison with Ni/mayenite B-wi and Ni/mayenite H-wi as evidenced by the TPR results. Although strong metal-support interactions are linked with better stability and higher carbon deposition tolerance, some studies[46,49] stated that the strong metal-support interactions could led to reduction of the amount of chemically active nickel and as a consequence to lower steam reforming conversions. The $\mathrm{k_{app}}$ values observed in the present work are comparable with the values obtained by Aznar et al. [26] who studied the steam reforming of a slip-stream taken from a fluidized bed gasifier on commercial nickel catalysts. It should be stressed that the authors [26] used a guard bed which reduced significantly the inlet tar concentration and likely change the composition of the tar, leaving mainly the most recalcitrant components such as benzene and toluene unaltered [50]. When the $\mathrm{k_{app}}$ values are computed considering the total wet gas flowrate instead of the N_2-free flowrate a reasonable agreement is found also with the values obtained by Świerczyński et al. [25] who studied the STR in the temperature range of 560 °C to 800 °C.

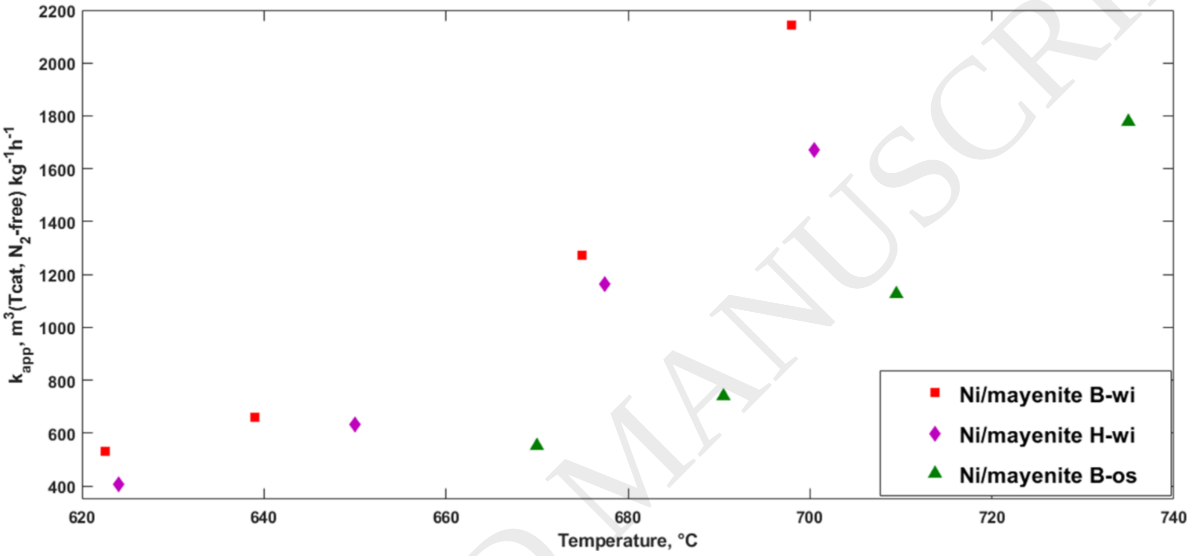

Fig. 10. k_{app} as a function of temperature for toluene steam reforming.

The kinetics parameter for Ni/mayenite B-wi, Ni/mayenite H-wi and Ni/mayenite B-os are listed in Table 5. Representation of the obtained $\mathrm{k_{app}}$ values according to the Arrhenius equation yielded a fair concordance, as shown in Fig. 11, with coefficient of determination values ≥ 0.98 (Table 5). The Activation energy values obtained for the three catalyst were similar, therefore, analogous chemical nature of nickel active sites is expected for all the catalyst. Activation energy values for the steam reforming reaction of toluene and benzene reported in the literature span from 36 to 230 kJ mol^{-1} [20,51–54]. The wide range of values are mainly due to difference in experimental conditions used as well as in the reactor model employed in the various studies. Mukai et al [51] separate the activation energy values in two temperature regions, namely low (≤ 530 °C) and high (≥ 530 °C) temperature. The authors [51] found activation energy values of 113 and 36 kJ mol^{-1} for the low and high temperature region, respectively, using a Ni/$La_{0.7}Sr_{0.3}AlO_{3-\delta}$ calcined at 800 °C. A change in the rate-determining step was thought to be the cause of the change in the activation energy value, the former change was attributed to the lattice oxygen contribution which was found to be important at temperatures ≥ 550 °C. In the present study no distinction was made between low and high temperature regions. Further kinetics studies are required to elucidate this argument.

Table 5
Kinetic parameter for STR.

	Ni/mayenite B-wi	Ni/mayenite H-wi	Ni/mayenite B-os
Ea (kJ mol^{-1})	134	137	145
A (m^3(Tcat) kg^{-1} h^{-1})	3.2 x 10^{10}	3.9 x 10^{10}	5.7 x 10^{10}
R^2	0.98	0.99	0.98

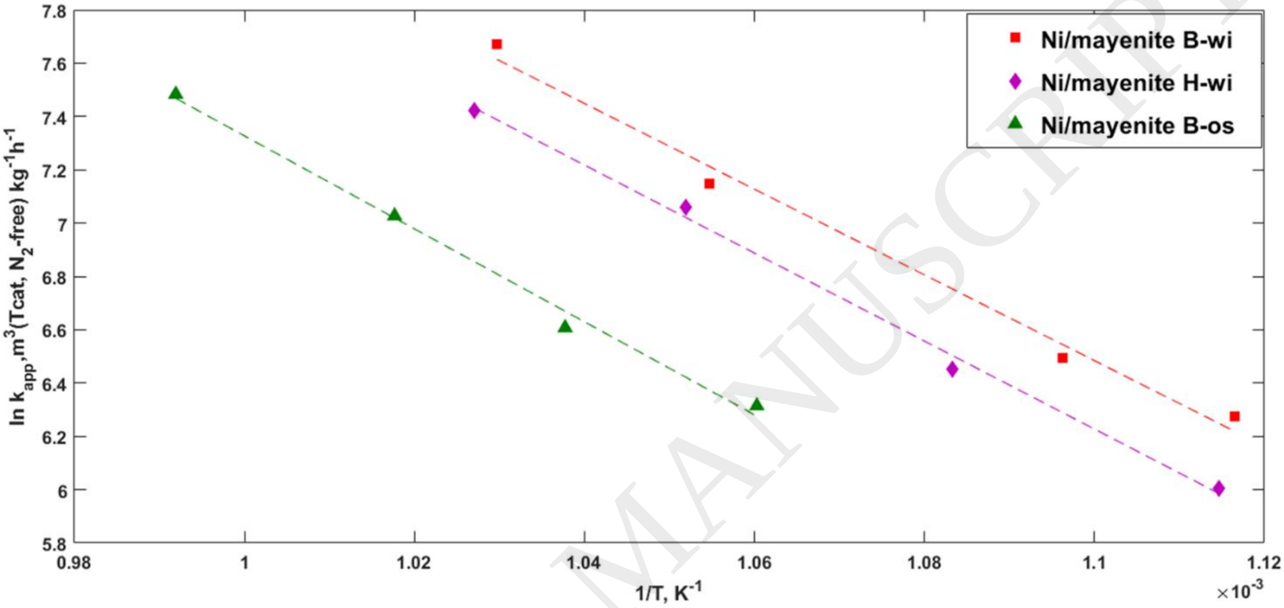

Fig. 11. Arrhenius representation for the k_{app} values of toluene steam reforming.

3.5. Characterization of used catalysts

The used catalysts were analyzed by X-ray diffraction and thermogravimetric oxidation (TPO) analysis in order to study the changes in their crystalline structure and to determine the carbon content formed during the catalytic test. The XRD patterns of the catalysts used in the steam reforming of toluene, are presented in Fig. 12A.

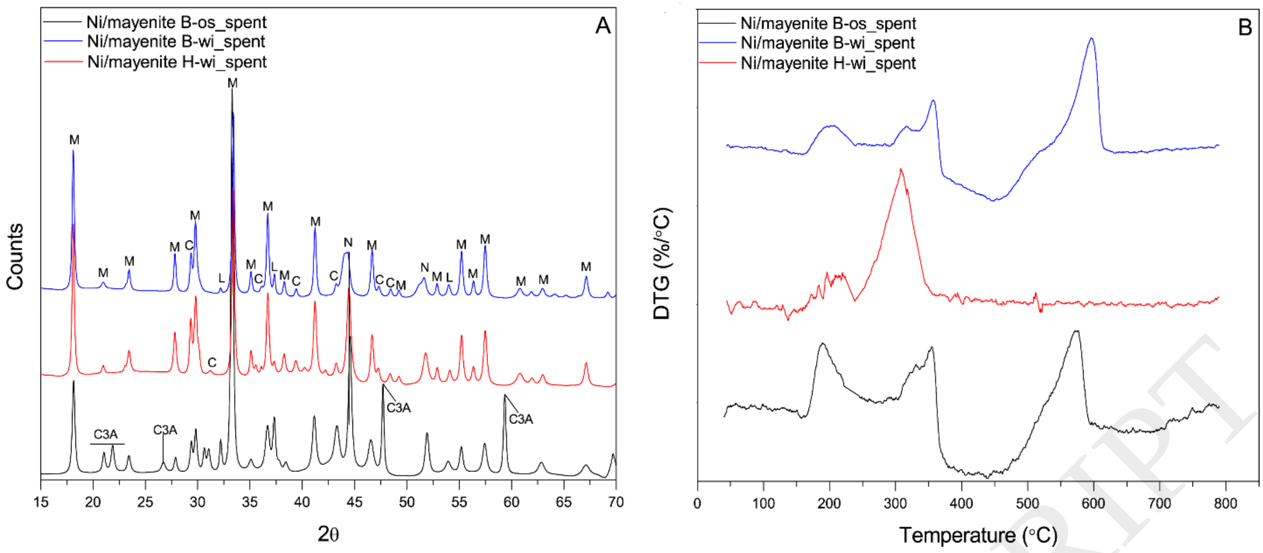

Fig. 12. (A) XRD patterns of used mayenite. M ($Ca_{12}Al_{14}O_{33}$); L (CaO); N (Ni); C ($CaCO_3$); C3A ($Ca_3Al_2O_6$). **(B)** DTG-TPO profiles of spent catalysts used in the steam reforming of toluene

The diffractograms of the spent samples are quite similar to those of the fresh samples, indicating that there were no significant structural changes caused by the exposure of the catalysts to the experimental conditions. Furthermore, no trace of carbon (crystalline phase) was detected on the catalysts after the reforming test. In the XRD pattern in addition to mayenite, CaO and Ni, also $CaCO_3$ (4.8% for Ni/mayenite B-os, 4.3% for Ni/mayenite B-wi and 11% for Ni/mayenite H-wi) was identified in all the catalysts, which is due to the CO_2 uptake by carbonation reaction on CaO during the steam reforming tests [41]. As previous reported, carbon dioxide removal by adsorption on a solid provide further heat to the reforming reaction that may lead to a higher hydrogen yield. [35]. Additionally, CO_2 sorption by the support could shift the WGS equilibrium reaction to the products side hence promoting the production of H_2 [36]. Furthermore for Ni/mayenite B-os $Ca_3Al_2O_6$ (41.5%) and NiO (7.8%) can be detected, which are a degradation phase of mayenite under humid condition [55] and unreduced Ni, respectively.

From the XRD analysis it was possible to determine the size of the metallic Ni crystallites in the used catalysts by applying the Scherrer equation to the (1 1 1) diffraction line at 2θ = 44.5°. The obtained values after the 6 h long test for the three catalysts are showed in Table 6

When the fresh and spent catalyst are compared, it is evident that the Ni/mayenite B-wi catalyst showed the largest Ni crystallites increment after use, which could be related to the fact that the isolated NiO species in this sample were reduced at the lowest temperature among the studied catalysts and this result is generally linked with high mobility of these species that upon reaction are also the most sensitive to agglomeration phenomenon. In the other cases, after the tests the increase of the Ni crystallite size was notably lower or almost unchanged, therefore it can be deduced that the partial deactivation of the Ni/mayenite H-wi during the 6-hour-long test was not related to the growth or agglomeration of Ni crystallites.

In Fig. 12B the DTG-TPO profiles corresponding to the different catalysts used are reported. The DTG profiles of the mayenite obtained by boehmite precursor are similar in the two used catalysts, showing three major peaks at around 200 °C, 350 °C and 600 °C. The percentage of deposited carbon corresponding to each peak is summarized in Table 6. As widely reported in the literature, the peak at 200 °C can be attributed to the carbon deposited on the metal active sites located on the surface of the catalyst [56,57]. The peak at 350 °C, much higher than the previous for Ni/mayenite B-wi, could be related to the oxidation of filamentous carbon species at the metal-support interface and the last high peak appearing at 600 °C could be associated to the oxidation of graphitic carbon species deposited on the mayenite support [28]. The oxidation profiles of the used catalysts obtained were similar, but with some differences in the intensity of the oxidation peaks. The Ni/mayenite B-wi catalyst showed higher oxidation peaks at 350 and 600°C compared to the Ni/mayenite B-os counterpart. Probably the bigger size of the Ni particles observed on the Ni/mayenite B-os catalyst (Table 6) lead to a reduction of the amount of filamentous carbon species, which typically forms on small Ni particles, as in Ni/mayenite H-wi [28]. Furthermore, in the case of Ni/mayenite B-wi the carbon deposits were mainly graphitic and thus less active, difficult to remove and responsible for catalyst deactivation. The Ni/mayenite H-wi showed a total amount of carbon deposited similar to that of Ni/ mayenite B with an intense peak corresponding to the filamentous carbon formation.

Table 6

Average crystallite size of the Ni particles and integrated areas of the TPO rate curves [58] on spent catalysts.

Catalysts	Crystal size (nm)	Carbon deposited at each temperature (%)		
		200	350	600
Ni/mayenite B-wi	31.52 (+ 10.8)	0.19	0.36	0.52
Ni/mayenite B-os	37.86 (- 0.04)	0.23	0.14	0.10
Ni/mayenite H-wi	27.02 (+ 5.3)	0.10	0.92	0

The total (sum) carbon deposited on the catalysts in mg of carbon per g of catalyst (mg of C g of cat.$^{-1}$) after a 6-h-long test at a temperature of 700 °C using toluene as tar model compound is summarized in Table 7. The peak at 200 °C was considered because this type of carbon can move from the metal to the interface of metal-support where further dehydrogenation and polymerization reactions are likely to occur [56], ultimately developing into filamentous or graphitic carbon. For comparison purposes, the obtained amount of carbon deposited values together with the main experimental conditions as well as the catalysts used and the nickel addition method of several studies taken from the literature are showed in Table 7. In general, the values for the carbon deposited on the catalysts are in agreement with the obtained values in this study as the above-mentioned catalysts were prepared with the aim of reduce the carbon deposition on the catalyst. Notably, the reported carbon deposited on the traditional Ni/α-Al_2O_3 catalyst was one order of magnitude higher than the values measured in the present study.

Table 7
Carbon deposited values in addition to the main experimental conditions applied in the corresponding experiment.

Catalysts	Nickel addition (method and loading)	Experimental conditions	Carbon deposited (mg of C g of cat.$^{-1}$)	Reference
Ni/$La_{0.7}Sr_{0.3}AlO_3$	Wet impregnation 5 wt. %	$C_7H_8/H_2O/Ar$ = 3/42/55 vol. % (total 100 ml min^{-1}); GHSV = 12000 h^{-1}; S/C = 2; T= 600 °C; ToS = 180 min.	57	[59]
Ni/α-Al_2O_3			431	
Ni/$LaAlO_3$			800	
Fe_3Ni_8/Palygorskite	Co-precipitation Ni = 8 wt. % Fe = 3 wt. %	C_7H_8 = 3000 ppm; cat. = 0.5 g; ToS = 100 min; T = 700 °C; S/C = 1.	12.2	[54]
		C_7H_8 = 3000 ppm; cat. = 0.5 g; ToS = 100 min; T = 700 °C; S/C = 1.5	10.9	
		C_7H_8 = 3000 ppm; cat. = 0.5 g; ToS = 100 min; T = 700 °C; S/C = 2	11.1	
Ni-Fe/Mg/Al	Co-precipitation during the support synthesis (one step) Ni = 12 wt. % Fe = 3.1 wt. %	$C_7H_8/H_2O/Ar$ = 0.75/8.9/26.8 mmol min^{-1}; T = 600 °C; ToS = 80 min; W/F = 0.014 g h mol^{-1}; S/C = 1.7	6.7	[47]
Ni/Mg/Al	Co-precipitation during the support synthesis (one step) Ni = 12 wt. %		79.4	
Ni/mayenite B-wi	Wet impregnation 10 wt. %	C_7H_8 = 47 g Nm^{-3}; GHSV = 73750 h^{-1}; W/F = 0.33 g h mol^{-1}; S/C = 5; ToS = 360 min; T = 700 °C	10.7	The present study
Ni/mayenite H-wi			10.2	
Ni/mayenite B-os	During the support synthesis (one-step) 10 wt. %		4.7	

4. Conclusion

Mayenite and Ni/mayenite catalysts were prepared using new procedures. Mayenite was synthetized starting from a slurry using hydroxides as precursors or alternatively from a gel of boehmite and calcium nitrate, each calcined at the suitable temperature determined by TGA-DSC. The slurry route appears of particular interest due to the lower cost of the precursors and the easier and faster preparation, however its calcination temperature was higher (ΔT= 300 °C) than in the case of gel route. Both procedures yielded materials with similar crystal structure but differed in their morphological structure. Ni addition was then synthesized both by wet impregnation and by direct inclusion of the precursors during the mayenite preparation. Neither $NiAl_2O_4$ spinel phase nor formation of solid solution between NiO and CaO were identified on the obtained catalysts. The Ni/mayenite catalysts were then tested on the steam reforming of toluene and pyrocatechol as tar model compounds. The catalyst obtained by direct inclusion of Ni precursor in the slurry route led to a poor dispersion of nickel and very low specific surface area values, resulting therefore in the absence of catalytic activity. Addition of nickel through the wet impregnation method led to analogous performances in all the conditions studied, despite morphological and structural differences. The lower activity observed with Ni/mayenite obtained by direct inclusion of Ni precursor in the gel route was attributed to its lower reduction degree, calculated after TPR characterization on the fresh catalyst. Degradation of the support during the experiments evidenced by the presence of $Ca_3Al_2O_6$ in the XRD analysis and/or the higher initial nickel crystal size calculated for this catalyst could also have contributed to the observed lower conversion values. Deactivation during toluene steam reforming of the Ni/mayenite catalysts produced by wet impregnation was ascribed to filamentous and graphitic carbon deposition for mayenite produced by the slurry route and the gel route respectively. Ni/mayenite obtained by direct inclusion of Ni precursor in the gel route showed slightly lower conversion values with respect to the catalysts prepared by the wet impregnation method but exhibited a promising carbon deposition tolerance in long duration test. This catalyst is promising due to its higher resistance to carbon deposition deactivation together with its simpler preparation method which foresees only one step.

Declarations of Interest

None

Acknowledgements

This research did not receive any specific grant from funding agencies in the public, commercial, or not-for-profit sectors.

References

[1] P. McKendry, Bioresour. Technol. 83 (2002) 55–63.

[2] R.M. Swanson, R.M. Swanson, Fuel 89 (2009) S11–S19.

[3] N. Abdoulmoumine, S. Adhikari, A. Kulkarni, S. Chattanathan, Appl. Energy 155 (2015) 294–307.

[4] L. Devi, K.J. Ptasinski, F.J.J.G. Janssen, Biomass and Bioenergy 24 (2002) 125–140.

[5] K. Maniatis, A.A.C.M. Beenackers, Biomass and Bioenergy 18 (2000) 1–4.

[6] W. Torres, S.S. Pansare, J.G. Goodwin, Catal. Rev. - Sci. Eng. 49 (2007) 407–456.

[7] J. Kopyscinski, T.J. Schildhauer, S.M.A. Biollaz, Fuel 89 (2010) 1763–1783.

[8] P. V. Aravind, W. De Jong, Prog. Energy Combust. Sci. 38 (2012) 737–764.

[9] C. Li, D. Hirabayashi, K. Suzuki, Appl. Catal. B Environ. 88 (2009) 351–360.

[10] E. Savuto, A. Di Carlo, K. Gallucci, S. Natali, E. Bocci, Fuel 194 (2017) 348–356.

[11] B. de Caprariis, M.P. Bracciale, P. De Filippis, A.D. Hernandez, A. Petrullo, M. Scarsella, Can. J. Chem. Eng. 95 (2017) 1745–1751.

[12] Z. Wang, Y. Pan, T. Dong, X. Zhu, T. Kan, L. Yuan, Y. Torimoto, M. Sadakata, Q. Li, Appl. Catal. A Gen. 320 (2007) 24–34.

[13] H. Hosono, K. Hayashi, K. Kajihara, P. V. Sushko, A.L. Shluger, Solid State Ionics 180 (2009) 550–555.

[14] H. Boysen, M. Lerch, A. Stys, A. Senyshyn, Acta Crystallogr. Sect. B Struct. Sci. 63 (2007) 675–682.

[15] A. Di Carlo, D. Borello, M. Sisinni, E. Savuto, P. Venturini, E. Bocci, K. Kuramoto, Int. J. Hydrogen Energy 40 (2015) 9088–9095.

[16] M. Valentini, G. Groppi, C. Cristiani, M. Levi, E. Tronconi, P. Forzatti, Catal. Today 69 (2001) 307–314.

[17] J. Gil, J. Corella, M.P. Aznar, M.A. Caballero, Biomass and Bioenergy 17 (1999) 389–403.

[18] J. Corella, A. Orío, P. Aznar, Ind. Eng. Chem. Res. 37 (1998) 4617–4624.

[19] S. Gražulis, D. Chateigner, R.T. Downs, A.F.T. Yokochi, M. Quirós, L. Lutterotti, E. Manakova, J. Butkus, P. Moeck, A. Le Bail, J. Appl. Crystallogr. 42 (2009) 726–729.

[20] D. Swierczynski, C. Courson, A. Kiennemann, Chem. Eng. Process. Process Intensif. 47 (2008) 508–513.

[21] K. Polychronopoulou, J.L.G. Fierro, A.M. Efstathiou, J. Catal. 228 (2004) 417–432.

[22] G.F. Froment, Chemie Ing. Tech. 46 (1974) 374–386.

[23] H.S. FOGLER, Chem. Eng. (2006).

[24] G.F. Froment, K.B. Bischoff, J. De Wilde, Chemical Reactor Analysis and Design, Third, John Wiley & Sons, Inc., 2011.

[25] D. Świerczyński, S. Libs, C. Courson, A. Kiennemann, Appl. Catal. B Environ. 74 (2007) 211–222.

[26] M.P. Aznar, M.A. Caballero, J. Gil, J.A. Martín, J. Corella, Ind. Eng. Chem. Res. 37 (1998) 2668–2680.

[27] A.S. Tolkacheva, S.N. Shkerin, S. V. Plaksin, E.G. Vovkotrub, K.M. Bulanin, V.A. Kochedykov, D.P. Ordinartsev, O.I. Gyrdasova, N.G. Molchanova, Russ. J. Appl. Chem. 84 (2011) 907–911.

[28] E. Savuto, R.M. Navarro, N. Mota, A. Di Carlo, E. Bocci, M. Carlini, J.L.G. Fierro, Fuel 224 (2018) 676–

686.

[29] M.P. Bracciale, B. De Caprariis, C. Bassano, P. De Filippis, P. Deiana, A.D. Hernandez, M. Scarsella, Chem. Eng. Trans. 65 (2018).

[30] M. Ruszak, S. Witkowski, P. Pietrzyk, A. Kotarba, Z. Sojka, Funct. Mater. Lett. 04 (2011) 183–186.

[31] M. Ruszak, S. Witkowski, P. Pietrzyk, A. Kotarba, Z. Sojka, Funct. Mater. Lett. 04 (2011) 183–186.

[32] M.G. Vincent, J.W. Jeffery, Acta Crystallogr. Sect. B Struct. Crystallogr. Cryst. Chem. 34 (1978) 1422–1428.

[33] W.W. Russel, J. Chem. Educ. 21 (1944) 52.

[34] C.S. Martavaltzi, A.A. Lemonidou, Ind. Eng. Chem. Res. 47 (2008) 9537–9543.

[35] M.R. Cesário, B.S. Barros, C. Courson, D.M.A. Melo, A. Kiennemann, Fuel Process. Technol. 131 (2015) 247–253.

[36] J. Phromprasit, J. Powell, S. Wongsakulphasatch, W. Kiatkittipong, P. Bumroongsakulsawat, S. Assabumrungrat, Int. J. Hydrogen Energy 41 (2016) 7318–7331.

[37] J.N. Kim, C.H. Ko, K.B. Yi, Int. J. Hydrogen Energy 38 (2013) 6072–6078.

[38] K. V. Manukyan, A.G. Avetisyan, C.E. Shuck, H.A. Chatilyan, S. Rouvimov, S.L. Kharatyan, A.S. Mukasyan, J. Phys. Chem. C 119 (2015) 16131–16138.

[39] A. Cabello, P. Gayán, L.F. De Diego, A. Abad, M.T. Izquierdo, J. Adánez, Appl. Catal. B Environ. 147 (2014) 980–987.

[40] J. Zhang, H. Xu, X. Jin, Q. Ge, W. Li, Appl. Catal. A Gen. 290 (2005) 87–96.

[41] A. Di Giuliano, F. Giancaterino, C. Courson, P.U. Foscolo, K. Gallucci, Fuel 234 (2018) 687–699.

[42] B. Abdullah, N.A. Abd Ghani, D.V.N. Vo, J. Clean. Prod. 162 (2017) 170–185.

[43] S. Sokolov, E. V. Kondratenko, M.M. Pohl, A. Barkschat, U. Rodemerck, Appl. Catal. B Environ. 113–114 (2012) 19–30.

[44] L. Zhang, X. Wang, B. Tan, U.S. Ozkan, J. Mol. Catal. A Chem. 297 (2009) 26–34.

[45] F. Arena, B.A. Horrell, D.L. Cocke, A. Parmaliana, N. Giordano, J. Catal. 132 (1991) 58–67.

[46] L. Pelletier, D.D.S. Liu, Appl. Catal. A Gen. 317 (2007) 293–298.

[47] M. Koike, D. Li, H. Watanabe, Y. Nakagawa, K. Tomishige, Appl. Catal. A Gen. 506 (2015) 151–162.

[48] D. Mukai, Y. Murai, T. Higo, S. Tochiya, T. Hashimoto, Y. Sugiura, Y. Sekine, Appl. Catal. A Gen. 466 (2013) 190–197.

[49] M.A. Goula, N.D. Charisiou, K.N. Papageridis, A. Delimitis, E. Pachatouridou, E.F. Iliopoulou, Int. J. Hydrogen Energy 40 (2015) 9183–9200.

[50] A.M. Steele, S. Poulston, K. Magrini-Bair, W. Jablonski, Catal. Today 214 (2013) 74–81.

[51] D. Mukai, S. Tochiya, Y. Murai, M. Imori, Y. Sugiura, Y. Sekine, Appl. Catal. A Gen. 464–465 (2013) 78–86.

[52] N. Kaisalo, P. Simell, J. Lehtonen, Fuel 182 (2016) 696–703.

[53] H. Depner, A. Jess, Fuel 78 (1999) 1369–1377.

[54] X. Zou, T. Chen, P. Zhang, D. Chen, J. He, Y. Dang, Z. Ma, Y. Chen, P. Toloueinia, C. Zhu, J. Xie, H. Liu,

S.L. Suib, Appl. Energy 226 (2018) 827–837.

[55] J.-P. Eufinger, A. Schmidt, M. Lerch, J. Janek, Phys. Chem. Chem. Phys. 17 (2015) 6844–6857.

[56] J. Ruixia, X. Zaiku, Z. Chengfang, C. Qingling, Appl. Catal. A Gen. 250 (2003) 209–220.

[57] C.L. Li, O. Novaro, X. Bokhimi, E. Muñoz, J.L. Boldú, J. a Wang, T. López, R. Gómez, N. Batima, Catal. Letters 65 (2000) 209–216.

[58] X. Xian, C. Ran, C. Nai, P. Yang, S. Zhao, L. Dong, Appl. Catal. A Gen. 547 (2017) 37–51.

[59] D. Mukai, S. Tochiya, Y. Murai, M. Imori, T. Hashimoto, Y. Sugiura, Y. Sekine, Appl. Catal. A Gen. 453 (2013) 60–70.